THE JOURNAL OF PHYSICAL CHEMISTRY B

ARTICLE

pubs.acs.org/JPCB

Conformational Disorder of Membrane Peptides Investigated from Solid-State NMR Line Widths and Line Shapes

Yongchao Su and Mei Hong*

Department of Chemistry, Iowa State University, Ames, Iowa 50011, United States

Supporting Information

ABSTRACT: A challenge in the application of solid-state NMR spectroscopy to membrane peptides and proteins is the relatively broad line widths compared to those for solution NMR spectra. To understand the linewidth contributions to membrane protein NMR spectra, we have measured the inhomogeneous and homogeneous line widths of several well-studied membrane peptides under immobilized conditions. ^{13}C T_2 relaxation times of uniformly ^{13}C-labeled residues show that the homogeneous line widths of the peptides are comparable to those of crystalline model compounds under identical ^{1}H decoupling and magic angle spinning conditions, indicating that the homogeneous line widths are determined by conformation-independent factors, including residual dipolar coupling, J-coupling, and intrinsic T_2 relaxation. However, the membrane peptides exhibit larger apparent line widths than the crystalline compounds, indicating conformational disorder. A cationic cell-penetrating peptide, the human immunodeficiency virus TAT, exhibits the largest apparent line widths, which are about five-fold larger than the homogeneous line widths, while the transmembrane helix of the influenza M2 peptide and the β-hairpin antimicrobial peptide PG-1 show moderately larger apparent line widths than the crystalline compounds. These results are consistent with the random coil nature of the TAT peptide, which contrasts with the intramolecularly hydrogen bonded M2 and PG-1. Cross peak line shapes of 2D double-quantum correlation spectra show that the conformational disorder can occur at the residue level and can result from three origins, lipid−peptide interaction, intrinsic conformational disorder encoded in the amino acid sequence, and side-chain rotameric averaging. A particularly important lipid−peptide interaction for cationic membrane peptides is guanidinium−phosphate ion pair interaction. Thus, NMR line widths and line shapes are useful for understanding the conformational disorder of membrane peptides and proteins.

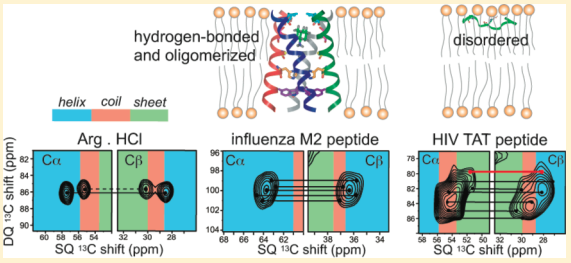

INTRODUCTION

Solid-state NMR (SSNMR) spectroscopy has become a powerful probe of the molecular structure and dynamics of insoluble biological macromolecules such as membrane proteins,[1,2] amyloid fibrils,[3−5] and cell walls.[6,7] A persistent challenge in structure determination of these biological solids is spectral resolution. While biomolecules in solution have narrow line widths due to their fast isotropic tumbling, solid systems, without such motion, exhibit broad NMR line widths due to the presence of orientation-dependent nuclear spin interactions such as chemical shift anisotropy (CSA) and dipolar coupling. Magic angle spinning (MAS)[8] and hetero- and homonuclear dipolar decoupling techniques[9−14] eliminate most of this orientational broadening. Nevertheless, residual dipolar couplings between protons and heteronuclei due to imperfect decoupling still contribute sizable line widths, and dipolar couplings between isotopically enriched ^{13}C spins broaden lines when MAS rates are insufficient. In addition, $^{13}C-^{13}C$ J-couplings are difficult to remove in directly detected ^{13}C spectra and thus contribute a fixed amount of linewidth. These coherent line broadening mechanisms are ameliorated by the use of higher magnetic fields,[15] faster MAS,[14,16] and reduction of the proton density by perdeuteration of proteins followed by H/D exchange.[17−19]

In contrast to the coherent linewidth contributions, an incoherent line broadening mechanism is transverse T_2 relaxation, which results from random fluctuations of local magnetic fields induced by molecular motion.[20,21] When motional rates are comparable to the strength of the dipolar decoupling field strengths or MAS rate, extreme line broadening occurs that abolishes the spectral intensity altogether. This intermediate time scale motional broadening has been studied in both small molecules[22,23] and membrane peptides.[24−26]

The third line broadening mechanism, which cannot be removed by radio frequency pulses or higher magnetic fields, is conformational disorder. Conformational distribution gives rise to multiple isotropic chemical shifts for each chemically unique nuclear spin in the same manner that chemically inequivalent spins cause different isotropic shifts. This inhomogeneous line broadening causes characteristic 2D correlation line shapes[27,28] and can give very broad peaks, even if the homogeneous line widths due to residual couplings and T_2 relaxation are small. The large difference between inhomogeneous and homogeneous line widths has

Received: May 29, 2011
Revised: July 29, 2011
Published: August 01, 2011

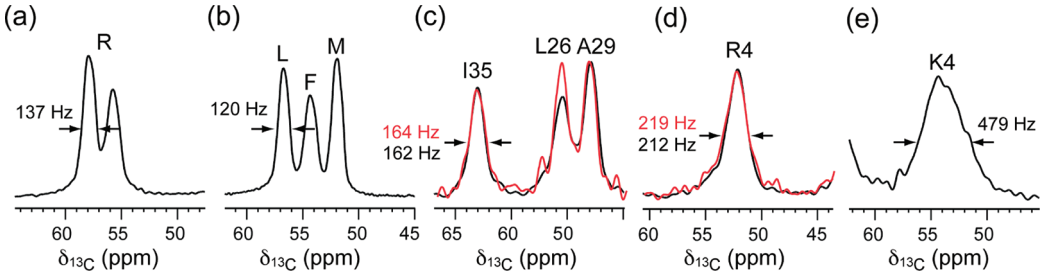

Figure 1. Representative Cα peaks from the ^{13}C CP-MAS spectra of (a) Arg·HCl at 296 K; (b) f-MLF-OH at 296 K; (c) LAGI-M2TM in viral membranes at 238 (black) and 293 K (red); and (d) Arg4-labeled PG-1 in POPE/POPG lipids at 238 (black) and 283 K (red). (e) Lys4-labeled TAT in POPE/POPG lipids at 238 K.

been exploited for designing *J*-coupling-based polarization transfer methods for solids.[29,30]

To date, the line broadening mechanisms of only a few biological solids have been investigated. These include cellulose in wood,[27,28,30] elastin,[31] and a crystalline tripeptide, formyl-Met-Leu-Phe-OH (f-MLF-OH).[32,33] No systematic study of the linewidth contributions of membrane-bound peptides and proteins has been reported. The amphipathic lipid bilayer surrounding membrane proteins[34] presents a complex anisotropic environment in which a distribution of lateral pressures and dielectric constants exists across the bilayer normal,[35] and abundant thermal disorder of the lipid chains is present. Thus, membrane-bound peptides and proteins have additional mechanisms of conformational disorder compared to crystalline molecules, globular proteins, and fibrous biopolymers. Figure 1 gives an example of the ^{13}C linewidth differences between crystalline compounds and membrane peptides. The 1D ^{13}C MAS spectra of two crystalline molecules, arginine hydrochloride (Arg·HCl) and f-MLF-OH, are compared with the spectra of three hydrated membrane peptides, the transmembrane (TM) domain of the influenza M2 protein (M2TM), the disulfide-bonded β-hairpin antimicrobial peptide PG-1, and the Arg-rich cell-penetrating peptide (CPP) HIV TAT. All amino acid residues examined are uniformly labeled in ^{13}C. The membrane peptide spectra were measured at a temperature (238 K) well below the gel-to-liquid-crystalline phase transition temperature to suppress any large-scale motion of the peptide backbone but not low enough to freeze methyl rotations or phenylene ring flips. At these temperatures, the line width contribution from intrinsic T_2 relaxation should be comparable between the crystalline compounds and membrane peptides. We applied the same ^{1}H decoupling field strength (71 kHz) and MAS rate (7 kHz) to maintain the same coherent line broadening contributions to the line widths. We found that arginine hydrochloride and f-MLF-OH exhibit Cα full widths at half-maximum (fwhm) of 120−140 Hz, M2TM and PG-1 show modestly larger Cα line widths of 160−210 Hz, while TAT exhibits a very large linewidth of ∼480 Hz. Thus, these membrane peptides exhibit varying degrees of static conformational disorder that is additional to the crystalline model compounds. Among the three membrane peptides, the line widths of M2TM and PG-1 are largely independent of temperature between 238 and 293 K (Figure 1c,d), whereas TAT has strikingly narrower line widths at ambient temperature due to near-isotropic motion, as described recently.[36]

In this work, we investigate the line broadening mechanisms of these representative membrane peptides by measuring the apparent and homogeneous line widths and by analyzing line shapes in 2D correlation spectra.[37] We measured these line widths at the moderate low temperature of 238 K, where the peptide backbones are immobilized in the gel phase of the membranes. The low-temperature linewidth is interesting for both technological and structural reasons because an increasing number of solid-state NMR experiments now utilize low temperature to enhance the spectral sensitivity[38] and to elucidate protein folding pathways.[39] Understanding the origins of membrane protein line broadening is thus important for developing new NMR methods to enhance spectral resolution and sensitivity and for harvesting the inherent structural information in the NMR line widths and line shapes. Our experiments reveal several mechanisms of conformational disorder that contribute to the inhomogeneous line widths and shed light on the relationship between dynamic exchange at physiological temperature and static conformational distribution at low temperature.

MATERIALS AND METHODS

Sample Preparation. All phospholipids, including POPE, POPG, DMPC, DPPC, DPPE, and egg sphingomyelin (SPM) and cholesterol, were purchased from Avanti Polar Lipids and used without further purification. Uniformly ^{13}C,^{15}N-labeled Arg·HCl was purchased from Sigma-Aldrich. Fmoc-protected uniformly ^{13}C,^{15}N-labeled amino acids were either prepared in house[40] or purchased from Sigma-Aldrich and Cambridge Isotope Laboratories. All peptides, including PG-1 (RGGRLCYCRRRFCVCVGR), the CPP domain of the HIV TAT protein (residues 48−60, GRKKRRQRRRPPQ), and M2TM (residues 22−46, SSDPLVVAASIIGILHLILWILDRL), were synthesized using Fmoc chemistry and purified by HPLC.

Hydrated proteoliposomes were prepared in aqueous solution as described before.[41,42] Lipids were mixed in chloroform and dried under nitrogen gas. The lipid film was redissolved in cyclohexane and lyophilized to remove trace organic solvent. The lipid vesicles were prepared by suspending the dry powder in phosphate buffer and freeze−thawed for six cycles. For the water-soluble PG-1 and TAT, the peptide solution was directly added to the lipid vesicle solution and incubated overnight before ultracentrifugation. For the insoluble M2TM, the peptide was reconstituted into lipid bilayers by dialysis using octyl-β-D-glucopyranoside.[41] All proteoliposomes have peptide/lipid molar ratios of 1:15 or 1:12.5 and were hydrated to ∼40% by mass using a pH 7.0 or 7.5 phosphate buffer.

All peptides contain uniformly ^{13}C- and ^{15}N-labeled residues. One PG-1 sample contained labeled Gly3 and Leu5, while another PG-1 sample contained labeled Arg4. Both samples were incorporated into POPE/POPG (3:1) membranes. One

M2TM sample contained labeled Val27, Ser31, Gly34, and Asp44 (VSGD-M2TM) and was reconstituted into DMPC bilayers. Another M2TM sample contained Leu26, Ala29, Gly34, and Ile35 labels (LAGI-M2TM) and was reconstituted into a virus-mimetic membrane consisting of DPPC, DPPE, SPM, and cholesterol (6:6:4.5:6.4). Two TAT samples containing a Lys4 label and an Arg8 label were bound to POPE/POPG (8:7) membranes.

Solid-State NMR Experiments. All solid-state NMR experiments were carried out on a Bruker DSX-400 spectrometer (Karlsruhe, Germany) operating at Larmor frequencies of 400.49 MHz for ^{1}H, 100.70 MHz for ^{13}C, and 40.58 MHz for ^{15}N. A double-resonance MAS probe tuned to ^{13}C/^{1}H or ^{15}N/^{1}H modes was used. A Kinetics Thermal System XR air-jet sample cooler (Stone Ridge, NY) was used for cooling samples using dry air or nitrogen gas as the input. Sample temperatures were direct readings from the thermocouple and were estimated to be within 1 °C of the true temperature due to the moderate MAS rates (<8 kHz) of all experiments. ^{13}C and ^{15}N chemical shifts were externally referenced to the α-glycine ^{13}CO resonance at 176.49 ppm on the TMS scale and ^{15}N-acetylvaline (NAV) at 122.0 ppm on the NH_3 scale, respectively.

One-dimensional ^{13}C and ^{15}N cross-polarization (CP) MAS spectra were measured using CP contact times of 0.5−1.5 ms. T_2 relaxation times were measured using the Hahn-echo experiment[43] under 7 kHz MAS. The temperature was 238 K for membrane peptides and 296 K for crystalline model compounds. ^{1}H TPPM decoupling[9] at 71.4 kHz was applied during detection. An acquisition time of ∼17 ms, which was sufficiently long to avoid truncation of the time signal, was used for most membrane peptides.

1D CP-MAS or 1D double-quantum (DQ) filtered MAS spectra were measured to extract the apparent ^{13}C linewidth as a function of temperature. The DQ experiment suppresses the natural abundance lipid ^{13}C signals and gives well-resolved peptide ^{13}C signals. No apodization was applied to the time signals when reading off the apparent line widths. In a few cases where two peaks partially overlap, we obtained the fwhm as twice the half width at half-maximum. For 2D correlation spectra, modest line broadening was used, as indicated in the figure caption. The SPC-5 sequence[44] was used to recouple the ^{13}C−^{13}C dipolar coupling in the DQ experiments. All DQ spectra were measured under 5333 Hz MAS. The 2D DQ dipolar INADEQUATE experiment[37] correlates mostly directly bonded carbon signals due to the short DQ mixing time used and the fact that the one-bond ^{13}C−^{13}C dipolar coupling is 5-fold stronger than two-bond couplings. In our experience, the dipolar INADEQUATE experiment has higher sensitivity than the *J*-coupling analogue.[30]

RESULTS

We chose three membrane peptides with different secondary structures and dynamics to examine the conformational dependence of SSNMR line widths and line shapes. The TM domain of the influenza M2 protein forms a four-helix bundle in the virus envelope and conducts protons for the virus life cycle.[45−47] The antimicrobial peptide PG-1 is a disulfide-linked β-hairpin[48,49] that associates into β-barrels in anionic lipid membranes[42,50,51] to kill bacterial cells. The cell-penetrating peptide, TAT, from HIV crosses the membrane of eukaryotic cells to transport molecular cargo.[52,53] Both PG-1 and TAT are cationic due to a large fraction of Arg residues in their amino acid sequences,[34] while M2TM is mostly hydrophobic.[47,54] The line widths of Arg4 and Arg11 in PG-1 have been reported before.[55]

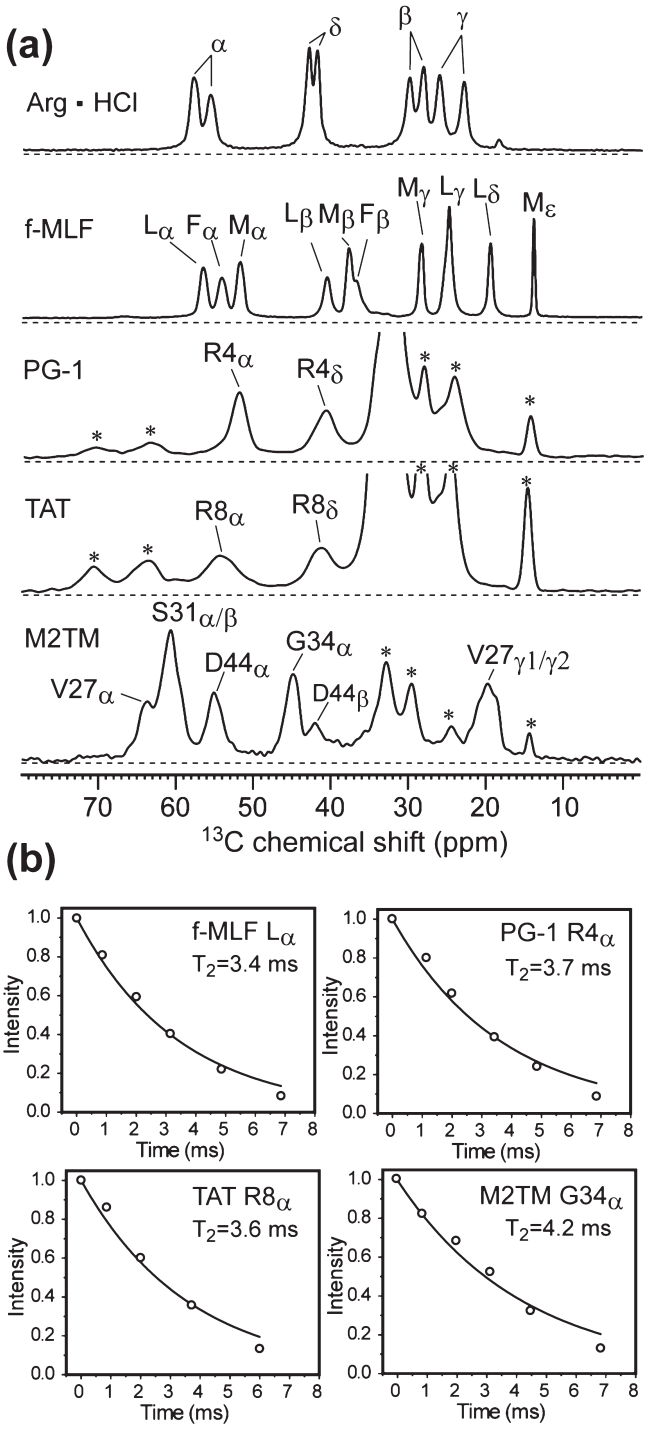

Figure 2. ^{13}C CP-MAS spectra and T_2 relaxation decays. (a) Representative ^{13}C CP spectra of Arg·HCl, f-MLF-OH, Arg4-labeled PG-1 in POPE/POPG membranes, Arg8-labeled TAT in POPE/POPG bilayers, and VSGD-M2TM in DMPC bilayers. Asterisks denote lipid ^{13}C peaks. Experiments were conducted at 293 K for the model compounds and at 238 K for the membrane peptides. (b) Representative fittings of exponential T_2 decays, measured under 7 kHz MAS and 71 kHz ^{1}H TPPM decoupling.

Table 1. ^{13}C Apparent (Δ^*) and Homogeneous (Δ) Line Widths of ^{13}C, ^{15}N-Labeled Compounds Obtained from 1D ^{13}C Spectra and T_2 Measurements, Respectively

peptide	site	CH_n	Δ^* (Hz)	Δ (Hz)	Δ^*/Δ
f-MLF-OH	L Cα	CH	120	93	1.3
	F Cα	CH	140	96	1.5
	M Cα	CH	116	78	1.5
	L Cγ	CH	90	64	1.4
	L Cβ	CH_2	112	98	1.1
	M Cβ	CH_2	106	68	1.6
	M Cγ	CH_2	73	43	1.7
	L $C\delta_{1/2}$	$(CH_3)_2$	64	47	1.4
Arg·HCl	R Cα	C	75	45	1.7
	R Cβ	CH	137	102	1.3
	R Cα	CH_2	112	70	1.6
	R Cβ	CH_2	125	95	1.3
	R Cγ	CH_2	125	99	1.3
M2TM	G34 Cα	CH_2	158	75	2.1
	V27 Cβ	CH	178	116	1.5
	D44 Cα	CH	167	89	1.9
	D44 Cβ	CH_2	180	105	1.7
PG-1	R4 Cζ	C	187	49	3.8
	R4 Cα	CH	215	86	2.5
	L5 Cα	CH	160	90	1.8
	R4 Cδ	CH_2	290	97	3.0
TAT	R8 Cζ	C	212	51	4.3
	K4 Cα	CH	479	100	4.8
	R8 Cα	CH	506	89	5.7
	R8 Cδ	CH_2	358	100	3.6
	K4 Cε	CH_2	354	145	2.4

Immobilized Membrane Peptides Have Similar Homogeneous Line Widths As Crystalline Compounds. We measured the ^{13}C T_2 relaxation times using the Hahn-echo experiment. The echo-detected T_2 gives the homogeneous linewidth (Δ) according to $\Delta = 1/\pi T_2$. In this work, we use the term homogeneous linewidth to denote the linewidth caused by both residual couplings and true T_2 relaxation because the two effects cannot be separated without infinitely strong ^1H decoupling, very fast MAS, and *J*-decoupling. The *J*-coupling results from the fact that the crystalline compounds and the examined residues in the membrane peptides are all uniformly labeled in ^{13}C, and neither MAS nor the hard-pulse spin−echo experiment removes $^{13}C-^{13}C$ *J*-coupling. Thus, two- and three-spin $^{13}C-^{13}C$ *J*-couplings contribute a fixed amount of 50−80 Hz to the ^{13}C homogeneous line widths. The apparent linewidth (Δ^*) read off from the fwhm of the spectral peaks includes both the homogeneous contribution and the inhomogeneous contribution and translates to an apparent T_2 relaxation time (T_2^*) according to $\Delta^* = 1/\pi T_2^*$. All spectra were measured at a magnetic field of 9.4 T and all ^{13}C T_2 relaxation times were measured under a ^1H decoupling field strength of 71 kHz. Stronger ^1H decoupling will give narrower Δ, while higher magnetic fields will result in larger apparent line widths Δ^*(in frequency units) due to the field dependence of the chemical shift.

Figure 2a shows the aliphatic region of the ^{13}C CP-MAS spectra of the crystalline compounds and the immobilized membrane peptides. Only resolved ^{13}C signals were used to report the T_2 values. Arginine hydrochloride shows two peaks for each ^{13}C site due to two inequivalent molecules in the asymmetric unit cell.[56,57] Representative T_2 decays are shown in Figure 2b. All data fit to single-exponential decays with time constants of 3−4 ms, indicating that the *J*-coupled ^{13}C homogeneous line widths are ∼100 Hz (∼1.0 ppm) for both the crystalline compounds and the hydrated membrane peptides under the conditions of the experiments.

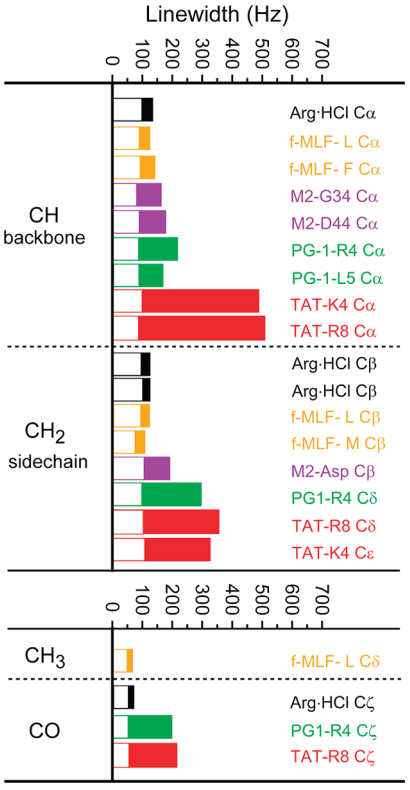

Figure 3. Summary of the ^{13}C apparent line widths (Δ^*, filled bars) and homogeneous line widths (Δ, open bars) of CH_n (n = 0−3) in crystalline compounds and membrane peptides.

Table 1 lists Δ and Δ^* of all measured sites, distinguished by their numbers of directly bonded protons. For Cα, the homogeneous line widths of all samples range from 75 to 100 Hz (0.75−1.0 ppm), irrespective of the crystalline or membrane-bound nature of the samples. At stronger ^1H decoupling fields, the Δ values decrease modestly[16,30,58] (Table S1, Supporting Information). In comparison, the membrane peptides exhibit larger Δ^* than crystalline compounds. For Cα, the membrane peptide Δ^* ranges from 160 to 500 Hz, while the model compound Δ^* spans 110−140 Hz. The Δ^*/Δ ratio is an indicator of the conformational heterogeneity of the samples;[30] larger conformational disorder gives multiple uncorrelated chemical shift frequencies, whose homogeneous linewidth can be much smaller. Table 1 shows that the two crystalline compounds have Cα Δ^*/Δ ratios of 1.3−1.5; M2TM and PG-1 Cα have moderately larger Δ^*/Δ ratios of 1.8−2.5. In contrast, TAT has large Δ^*/Δ ratios of 5−6, indicating severe conformational disorder. The TAT peptide disorder approaches the reported Δ^*/Δ ratios of 5−17 for cellulose in wood, measured under 10 kHz MAS and 100 kHz ^1H decoupling.[30]

Side-chain CH_2 carbons show similar trends of Δ^* among the different samples, with TAT exhibiting the largest Δ^*. Figure 3 plots the homogeneous (open bars) and apparent (filled bars)

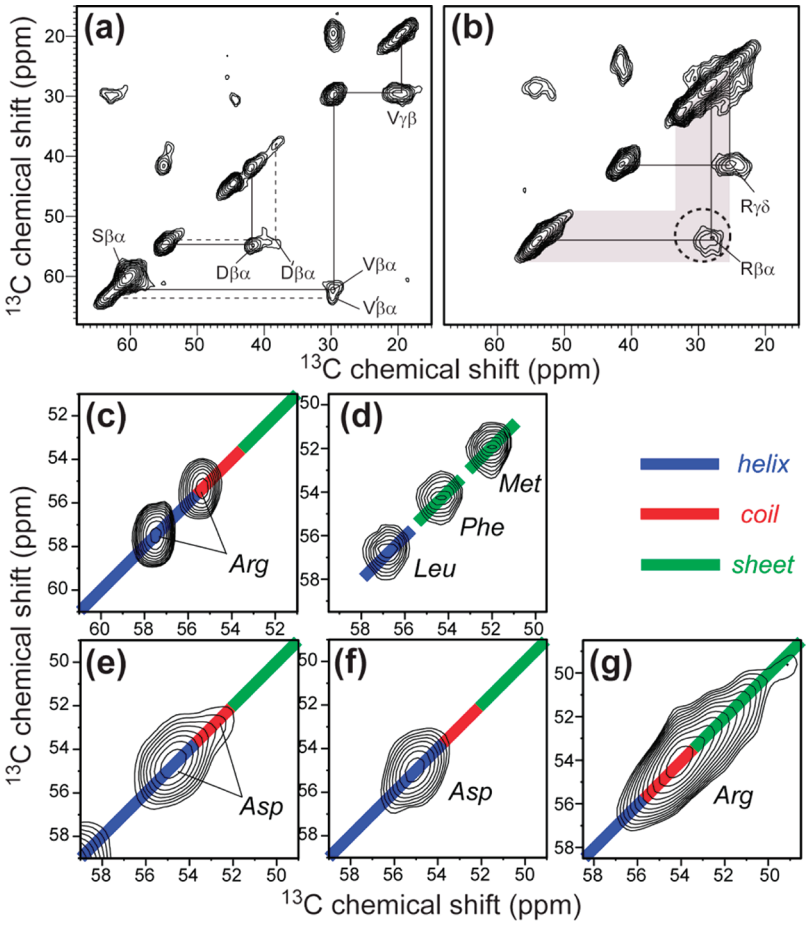

Figure 4. Conformational dispersion of membrane-bound peptides revealed by 2D DQ filtered correlation spectra. (a) VSGD-M2TM in DMPC membranes at 238 K. (b) Arg8-labeled TAT in POPE/POPG membranes at 238 K. (c) Cα region of Arg·HCl at 296 K. (d) f-MLF-OH at 296 K. (e) VSGD-M2TM in DMPC membranes at 238 K. (f) VSGD-M2TM in viral membranes at 273 K. (g) Arg8-labeled TAT in POPE/POPG lipids at 238 K. Colors indicate the chemical shift ranges of α-helix (blue), random coil (red), and β-sheet (green) conformations.

line widths of the different carbons, organized according to CH, CH_2, CH_3, and quaternary carbons. The average homogeneous linewidth is the smallest for quaternary carbons, 45−51 Hz, as expected because of their weak ^{1}H dipolar coupling. Methine and methylene carbons show similar homogeneous line widths of ∼90 Hz. CH_2 carbons are expected to have larger Δ due to stronger residual ^{1}H dipolar couplings; however, many CH_2 groups examined here are from the amino acid side chains, whose mobility may attenuate the ^{1}H−^{13}C dipolar coupling.

The crystalline Arg·HCl have smaller Δ*/Δ ratios (1.3−1.7) than arginines in membrane-bound PG-1 and TAT (2.5−5.7). Arg4 in PG-1 also has 1.4 times larger Δ*/Δ than its neighboring residue Leu5. Another Arg in PG-1, Arg11, exhibits an even larger Cα linewidth Δ* of 460 Hz (not shown). Thus, Arg in membrane peptides experiences additional line broadening mechanisms that are absent in the crystalline environment and have larger local conformational disorder than neutral residues in the peptides. ^{13}C−^{31}P distance measurements showed that many Arg-rich membrane peptides form guanidinium−phosphate complexes with lipid head groups[34,36,50,51,59] to carry out their functions. Thus, we attribute the larger line widths of Arg's in membrane peptides to this specific peptide−lipid interaction.

Conformational Disorder of Membrane Peptides from 2D Correlation Spectra. The 1D ^{13}C spectra above show strong variations in the apparent line widths (Δ*/Δ) of the three membrane peptides. M2TM has the smallest Δ*, while the cationic residues in PG-1 and TAT have the largest Δ*. To gain insight into the nature of the conformational disorder represented by these line widths, we measured the 2D DQ filtered single-quantum (SQ) correlation spectra of these peptides. Figure 4 shows the aliphatic regions of representative 2D spectra. Database chemical shift ranges for α-helical, β-sheet, and random coil structures are distinguished by color. Peak assignments are based on the connectivity patterns as well as literature reports.[60,61] Along the spectral diagonal, the crystalline compounds exhibit round line shapes, while the membrane peptide line shapes are elongated. The latter is a sign of the inhomogeneous nature of the line broadening, where the homogeneous linewidth is reflected by the narrower linewidth in the direction perpendicular to the spectral diagonal. The specific conformations of the residues can be gleaned from the chemical shifts spanned by the Cα peaks. One of the two Cα peaks of Arg·HCl resonates at a coil/sheet chemical shift, while the other Cα signal resonates at the α-helical frequency. In f-MLF-OH, the three Cα chemical shifts correspond to conformations that are consistent with the results of direct (ϕ,ψ) torsion angle measurements.[62] For M2TM, the D44 Cα peak spans the α-helical, and the coil chemical shifts for the peptide for a

dx.doi.org/10.1021/jp205002n |J. Phys. Chem. B 2011, 115, 10758–10767

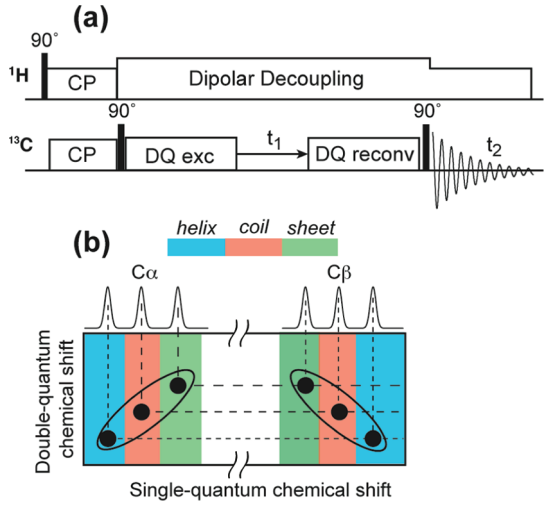

Figure 5. (a) Pulse sequence of the dipolar INADEQUATE experiment.[37] (b) Predicted INADEQUATE Cα−Cβ cross peak line shapes if a residue has well-defined secondary structures within each molecule but the secondary structure varies from one molecule to another.

DMPC-bound sample at 238 K but becomes only α-helical when the peptide is bound to a virus-mimetic membrane at 273 K (Figure 4e,f). This conformational difference is mostly due to the membrane composition and not the temperature difference because viral-membrane-bound M2TM shows the same line widths between 238 and 293 K (Figure 1c).[63] Arg8 Cα of TAT exhibits the largest chemical shift distribution among all sites examined, with Δ^* more than two times larger than those of M2TM.

To examine how the lineshape of one carbon is correlated with the lineshape of its directly bonded carbon, we measured the 2D INADEQUATE spectra, which correlate DQ chemical shifts with SQ frequencies[37,64] (Figure 5a). The indirect dimension of the spectrum represents the sum of the chemical shifts of the two coupled ^{13}C spins. Compared to the SQ correlation spectra shown in Figure 4, the INADEQUATE experiment has the advantage that it not only suppresses natural abundance ^{13}C signals but also removes the spectral diagonal so that carbons with similar chemical shifts are well resolved. Figure 5b depicts the hypothetical line shapes expected for a Cα−Cβ spin pair. For conformationally disordered proteins, multiple cross peaks are expected for each ^{13}C pair. It is well-known that Cα and Cβ have opposite signs for their secondary-structure-dependent chemical shifts.[65,66] For example, in α-helices, Cα has larger chemical shifts than random coil values, while Cβ has smaller chemical shifts than random coil values. As a result, if each molecule exhibits a well-defined conformation but the structure varies from one molecule to another, then the pair of Cα−Cβ cross peaks should be elongated and tilted in opposite directions in the INADEQUATE spectrum (Figure 5b). On the other hand, if each molecule already dynamically samples a range of conformations at high temperature and the ensemble is frozen at low temperature, then a Cα chemical shift can correlate with multiple Cβ chemical shifts and vice versa, leading to round line shapes for the pair of broadened cross peaks. Finally, a conformationally ordered ensemble of molecules should exhibit narrow line widths due to only T_2 relaxation and residual dipolar and J couplings. If the DQ ^{13}C T_2 can be approximated as the sum of the two SQ T_2's,[67] then the pair of cross peaks should exhibit elliptical line shapes with the long axis parallel to the ω_1 axis.

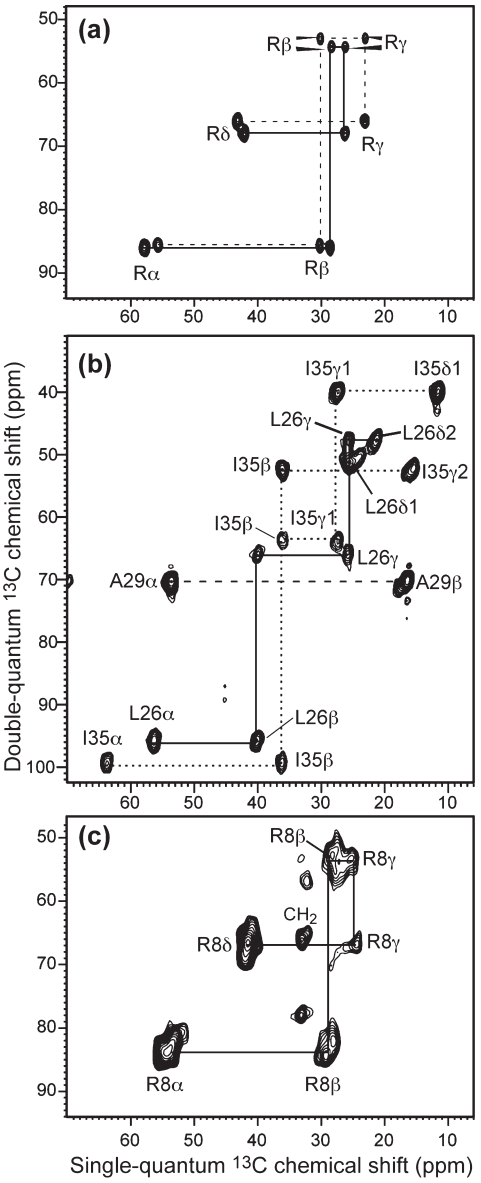

Figure 6. 2D ^{13}C INADEQUATE spectra of (a) Arg·HCl at 296 K, (b) viral-membrane-bound LAGI-M2TM at 238 K, and (c) Arg8-labeled TAT in POPE/POPG membranes at 238 K. All spectra were measured under 5333 Hz MAS and 71 kHz ^{1}H TPPM decoupling. Gaussian multiplication was applied to both dimensions with LB/GB values of −3/0.1, −7/0.07, and −15/0.04 for (a), (b), and (c), respectively. The single-quantum Cα line widths of Arg hydrochloride, M2TM Ile35, and TAT Arg8 are 126, 138, and 360 Hz, respectively.

Figure 6 shows three representative 2D INADEQUATE spectra. The Arg·HCl spectrum resolves two sets of ^{13}C connectivities for the two inequivalent molecules (Figure 6a) and shows oval line shapes that are parallel to the ω_1 axis for each pair of cross peaks. This lineshape is consistent with the ordered nature of this crystalline compound. The viral-membrane-bound M2TM has modestly larger line widths than arginine hydrochloride, but most pairs of cross peaks exhibit oval line shapes with the long axis parallel to the ω_1 axis, with the exception of the side-chain carbons of Ala29 and Leu26, which show tilted line shapes indicative of side-chain disorder (Figure 6b). Membrane-bound TAT exhibits by far the broadest peaks with ill-defined

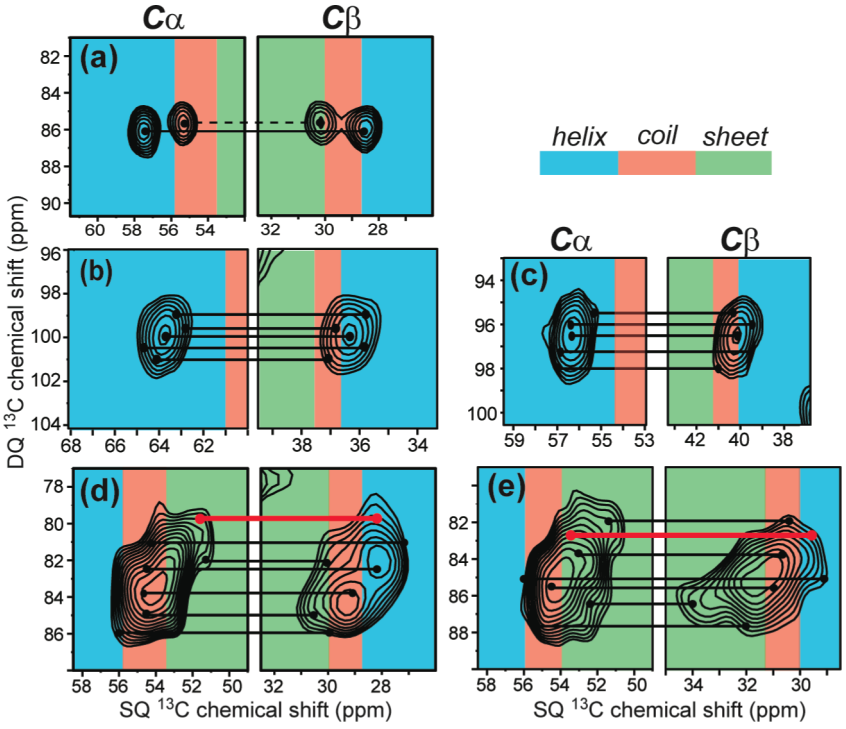

Figure 7. Amplified Cα−Cβ regions of the INADEQUATE spectra. (a) Arg·HCl at 296 K. (b) Ile35 of viral-membrane-bound M2TM at 238 K. (c) Leu26 of viral-membrane-bound M2TM at 238 K. (d) Arg8 of TAT in POPE/POPG bilayers at 238 K. (e) Lys4 of TAT in POPE/POPG bilayers at 238 K. Helix, coil, and sheet chemical shift regions are shaded in blue, red, and green, respectively. Selected correlated Cα−Cβ positions are connected by lines to guide the eye. Sheet−helix chemical shift correlations are colored by red lines.

shapes (Figure 6c). Figure 7 zooms in the Cα−Cβ region of the 2D spectra to examine the backbone conformational distribution. Characteristic chemical shift ranges for α-helix, β-sheet, and random coil[68] are shaded in blue, green, and red, respectively. The two dimensions of the spectra are drawn with the same ppm range per unit length to reflect the relative line widths of the DQ and SQ dimensions. In Arg·HCl (Figure 7a), one pair of Cα−Cβ cross peaks corresponds to the α-helical conformation, while the other pair falls in the coil/sheet secondary shift region. This is consistent with the crystal structure, which shows one molecule with (ϕ,ψ) angles of (−50°,−51°), corresponding to a helical backbone, while the other molecule has (ϕ,ψ) angles of (0°,−41°) outside of the helix or sheet regions of the Ramachandran diagram. The apparent line widths in the DQ dimension are 40−50 Hz smaller than the sum of the SQ line widths for the two crystalline model compounds due to the fact that DQ coherence commutes with the ^{13}C−^{13}C coupling so that the ω_1 linewidth is not broadened by ^{13}C−^{13}C J-coupling.

In viral-membrane-bound M2TM, the Ile35 and Leu26 line shapes show moderate conformational disorder (Figure 7b,c); both Cα peaks fall well within the α-helical range, while the Cβ chemical shifts are found in both the helix and coil regions. In contrast, the TAT Lys4 and Arg8 peaks span all three secondary structures (Figure 7d,e). In addition to the expected coil−coil and sheet−sheet Cα−Cβ correlations (black lines), we observed β-sheet Cα shifts correlated with α-helical Cβ shifts (red lines). This random correlation creates tilted line shapes that differ from the case depicted in Figure 5b. Thus, these residues adopt (ϕ,ψ) torsion angles far from the canonical secondary structures in some of the molecules. This indicates large conformational distributions at the residue level, which suggests dynamically interconverting conformers at physiological temperature.

Side-Chain Conformational Disorder. An inhomogeneously broadened peak can result from a continuous distribution of many frequency components or the overlap of a few discrete peaks. Bajaj et al. studied the temperature-dependent line widths of the solvent-free microcrystalline f-MLF-OH and found discrete peaks per carbon between 90 and 200 K.[69] They attributed the temperature-induced spectral changes to slowing down of the phenylene ring flips at low temperature, which affected the Met and Leu side-chain conformations.

We also observed temperature-dependent discrete side-chain disorder in PG-1. At 238 K, Arg4 of PG-1 in POPE/POPG membranes shows two Cβ peaks (29.5 and 33.1 ppm) correlated with the same Cα chemical shift (Figure 8a). When the temperature was increased to 283 K, a single Cβ peak was observed at the averaged position (31.7 ppm) of the two low-temperature chemical shifts (Figure 8b,c). Thus, Arg4 undergoes equal-population two-site exchange that is slow at 238 K but fast at 283 K. Because the PG-1 backbone is disulfide-bonded to be a robust β-hairpin and Arg4 Cα does not display this peak doubling, the nature of the conformational exchange is most likely side-chain rotameric averaging, as reflected by the low order parameters measured for this side chain at 283 K.[55] The existence of the side-chain conformational distribution is also consistent with the fact that the ^{13}Cζ−^{31}P distance between Arg4 guanidinium and lipid phosphates shows a distribution in the previously reported REDOR data.[51] Assuming a Gaussian distribution, we had obtained a best-fit distance of 5.7 Å with a distribution of 1.5 Å. The present observation of two discrete Cβ peaks suggests that the conformational distribution may be more accurately described

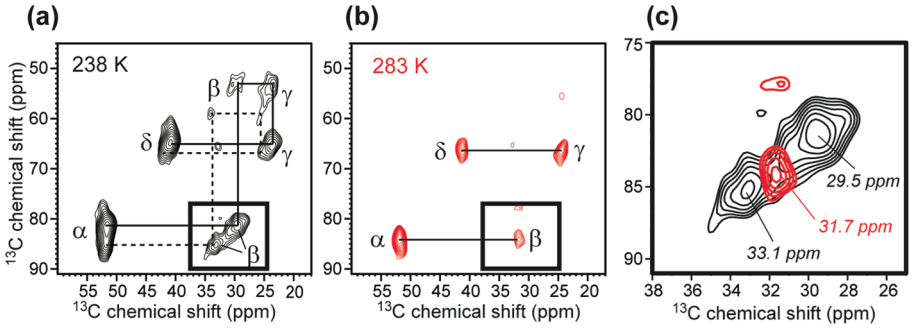

Figure 8. 2D ^{13}C INADEQUATE spectra of POPE/POPG-bound Arg4-labeled PG-1 at (a) 238 and (b) 283 K. (c) Enlarged region of the Cβ peak at the two temperatures.

as bimodal rather than a single Gaussian distribution. Indeed, the REDOR dephasing data can be equally well fit by a 1:1 combination of a short distance of 4.8 Å and a long distance of 8.5 Å (Figure S1, Supporting Information). The revised fitting, with one of the two distances being much shorter than the average distance of 5.7 Å from the single Gaussian fit, strengthens the model that the guanidinium−phosphate interaction is strong for membrane-bound PG-1.[50,51,70] Arg4 lies in the β-strand part of the peptide, far from the tip of the hairpin near the membrane surface. Thus, the fact that Arg4 guanidinium can approach lipid ^{31}P to 4.8 Å means that the guanidinium ions are very effective in dragging lipid head groups into the traditionally hydrophobic region of the bilayer, causing toroidal pore defects.

DISCUSSION

We measured the line widths and conformational distribution of the three membrane peptides at 238 K, a temperature at which all peptides are immobilized in the gel phase of their respective membranes but do not undergo any glass transition, which is a phenomenon largely observed in globular proteins at lower temperatures of 180−220 K.[32,71,72] The similar line widths of M2TM and PG-1 between 238 and 293 K (Figure 1c,d) also confirm that the conformational distribution of the peptides at 238 K is similar to the distribution at more moderate temperatures of the gel phase.

In the gel phase, all examined ^{13}C sites of the membrane peptides exhibit larger apparent line widths and Δ^*/Δ ratios than the crystalline compounds, indicating larger static disorder. On the other hand, the homogeneous line widths Δ are similar between the membrane peptides and the crystalline compounds, verifying the hypothesis that Δ is mainly dictated by intrinsic T_2 relaxation and residual dipolar and J-broadening.

Both 2D INADEQUATE line shapes and Δ^*/Δ ratios indicate that the three membrane peptides have different degrees of conformational disorder. M2TM and neutral residues in PG-1 have relatively small disorder, while cationic residues in PG-1 and TAT have much larger inhomogeneous broadening. These differences can be understood from the oligomeric structure and lipid interactions of these peptides. M2TM forms a water-filled tetrameric helical bundle[1,73−75] that is immobilized in the virus-mimetic membrane.[63] The interhelical interactions stabilize the peptide backbone, and the high viscosity of the cholesterol-rich viral membrane reduces the conformational plasticity of the helices.[63] The conformational landscape of M2TM has been investigated extensively. It is known that the peptide adopts several discrete "basis" conformations whose equilibria depend on the membrane composition, pH, and drug binding.[76,77] In the virus-mimetic membrane, a single dominant conformation was previously observed with small (ϕ,ψ) angle distributions,[76] consistent with the relatively narrow line widths seen in the 2D spectra here.

PG-1 is constrained by two disulfide bonds to adopt a well-defined β-hairpin structure.[78] In addition, it oligomerizes into a transmembrane β-barrel in the POPE/POPG membrane,[42] thus the peptide−peptide interaction should also reduce the conformational distribution. Countering this influence is the abundant peptide−lipid interactions, peptide−water interactions, and side-chain conformational averaging. Among these mechanisms, the guanidinium−phosphate salt bridge interaction appears to be the main contributor to line broadening, as reflected by the narrower line widths of neutral residues in PG-1 (Table 1).

The Arg residues of TAT also exhibit large inhomogeneous line broadening, but charge−charge interaction is not the dominant cause. Instead, the TAT amino acid sequence encodes for an intrinsic lack of a single conformation. The TAT protein from which the CPP domain is derived is an RNA-binding protein central for HIV replication and interacts with a variety of intracellular and extracellular molecules. Solution NMR studies have shown that the TAT protein does not have a fixed conformation in solution,[79] similar to a number of other intrinsically disordered proteins, which adopt specific structures only upon binding to substrates.[80] The current data show that the highly basic cell-penetrating domain of the TAT protein remains unstructured upon binding to the lipid membrane. The broad low-temperature Cα/Cβ peaks correlate with extremely narrow high-temperature peaks, both of which are centered at random coil chemical shifts[36] in several membrane compositions (Table S2, Supporting Information). Thus, TAT undergoes nearly isotropic motion and samples a large conformational space at high temperature, and the ensemble of conformations is captured by slow freezing. The nearly isotropic motion of the TAT structure gives rise to resolved ^{13}C−^{13}C J-splittings in the high-temperature spectra (Figure 9), even when the ^{1}H decoupling strength is weak (50 and 25 kHz). In DMPC/DMPG bilayers, the C−H order parameters for Cα and Cβ sites are only 0.15−0.18,[36,81] further confirming the dynamic nature of this peptide in the lipid bilayer.

We posit that the unstructured nature of the TAT peptide in the membrane is functionally important. By having no fixed conformation due to the lack of intramolecular H-bonds, TAT can better form transient intermolecular H-bonds with lipid phosphates and water to facilitate its translocation across the lipid bilayer.[36] The lack of a stable amphipathic conformation also prevents TAT from forming long-lasting hydrophobic interactions

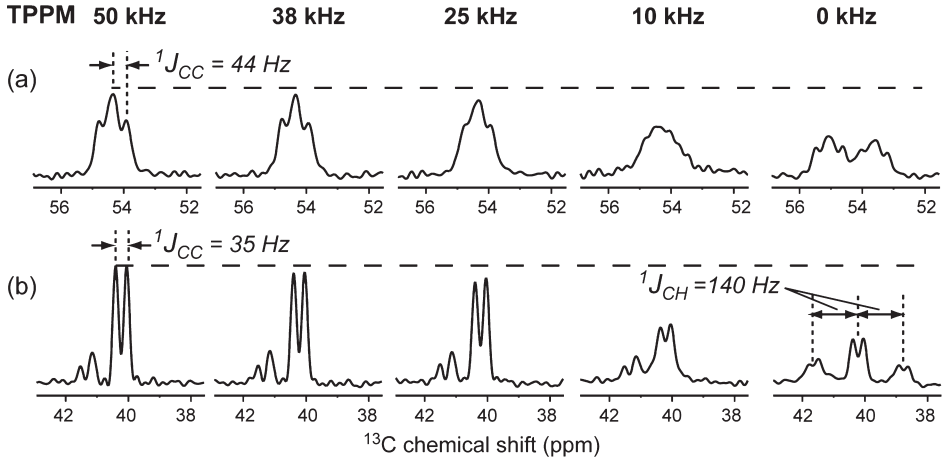

Figure 9. Cα (a) and Cε (b) peaks of Lys4-labeled TAT in POPE/POPG bilayers at 303 K. The spectra were measured by direct ^{13}C polarization under 5 kHz MAS with varying ^{1}H decoupling field strengths. (a) Cα peaks. (b) Cε peaks.

with the lipid bilayer, which would prohibit its membrane translocation activity.

The homogeneous line widths reported here are specific for the ^{1}H decoupling field strength of ∼70 kHz. Stronger ^{1}H decoupling lengthens the T_2 and decreases the homogeneous line widths.[82,83] As noted above, ^{13}C−^{13}C *J*-coupling and residual dipolar coupling also contribute a fixed amount to the homogeneous line widths of these uniformly ^{13}C-labeled residues. For comparison, the ^{15}N spins, without any *J*-coupling, show limiting homogeneous line widths of ∼10 Hz (0.25 ppm) for crystalline compounds (Table S3, Supporting Information). For singly ^{13}C-labeled crystalline compounds, the ^{13}C homogeneous line widths are 20−30 Hz for backbone Cα (Table S4, Supporting Information), much smaller than the line widths of uniformly ^{13}C-labeled samples.

CONCLUSIONS

We have investigated the conformational disorder of several membrane peptides by comparing their homogeneous and apparent line widths and by examining their 2D spectral line shapes. At low temperature, the membrane peptides exhibit similar homogeneous line widths as crystalline compounds, consistent with the origins of homogeneous line widths in residual coherent couplings and T_2 relaxation. However, membrane peptides exhibit larger apparent line widths than crystalline compounds, and the extent of the line broadening is a function of the peptide conformation. The largest apparent line widths are observed for nonoligomeric and cationic TAT due to its intrinsic near-random conformation and extensive peptide−lipid interaction. The main source of disordering peptide−lipid interactions in cationic membrane peptides is the guanidinium−phosphate interaction, which causes multiple side-chain conformations and distance distribution in addition to chemical shift distribution.

The current study indicates that strong peptide−peptide interactions through oligomerization (as for M2TM and PG-1) promote relatively homogeneous conformations, while extensive peptide−lipid interactions for monomeric peptides such as TAT cause larger line widths and conformational disorder. This insight may be useful for freeze-trapping experiments for studying protein folding intermediates[84] and protein photoreactions.[69,85] Low-temperature experiments have become increasingly important in biological SSNMR[39,84,86−88] due to the maturation of the dynamic nuclear polarization technique.[69,89] Our data indicate that the line widths of membrane proteins without strong charge interactions with lipids are not excessively broadened at temperatures down to about 230 K. Investigation of membrane protein line widths at even lower temperatures (to about 100 K) will further elucidate the applicability of DNP to membrane proteins.

ASSOCIATED CONTENT

Supporting Information. Line widths and REDOR data. This material is available free of charge via the Internet at http://pubs.acs.org.

AUTHOR INFORMATION

Corresponding Author

*Tel: 515-294-3521. Fax: 515-294-0105. E-mail: mhong@iastate.edu.

ACKNOWLEDGMENT

This work is funded by NIH grant GM66976 to M.H.

REFERENCES

(1) Cady, S., D.; Schmidt-Rohr, K.; Wang, J.; Soto, C. S.; Degrado, W. F.; Hong, M. *Nature* **2010**, *463*, 689.
(2) Lange, A.; Giller, K.; Hornig, S.; Martin-Eauclaire, M. F.; Pongs, O.; Becker, S.; Baldus, M. *Nature* **2006**, *440*, 959.
(3) Petkova, A. T.; Ishii, Y.; Balbach, J. J.; Antzutkin, O. N.; Leapman, R. D.; Delaglio, F.; Tycko, R. *Proc. Natl. Acad. Sci. U.S.A.* **2002**, *99*, 16742.
(4) Wasmer, C.; Lange, A.; Van Melckebeke, H.; Siemer, A. B.; Riek, R.; Meier, B. H. *Science* **2008**, *319*, 1523.
(5) Helmus, J. J.; Surewicz, K.; Nadaud, P. S.; Surewicz, W. K.; Jaroniec, C. P. *Proc. Natl. Acad. Sci. U.S.A.* **2008**, *105*, 6284.
(6) Cegelski, L.; O'Connor, R. D.; Stueber, D.; Singh, M.; Poliks, B.; Schaefer, J. *J. Am. Chem. Soc.* **2010**, *132*, 16052.
(7) Dick-Pérez, M.; Zhang, Y.; Hayes, J.; Salazar, A.; Zabotina, O. A.; Hong, M. *Biochemistry* **2011**, *50*, 989.
(8) Maricq, M. M.; Waugh, J. S. *J. Chem. Phys.* **1979**, *70*, 3300.
(9) Bennett, A. E.; Rienstra, C. M. A., M.; Lakshmi, K. V.; Griffin, R. G. *J. Chem. Phys.* **1995**, *103*, 6951.
(10) Fung, B. M.; Khitrin, A. K.; Ermolaev, K. *J. Magn. Reson.* **2000**, *142*, 97.
(11) Detken, A.; Hardy, E. H.; Ernst, M.; Meier, B. H. *Chem. Phys. Lett.* **2002**, *356*, 298.

(12) Sakellariou, D.; Lesage, A.; Hodgkinson, P.; Emsley, L. *Chem. Phys. Lett.* **2000**, *319*, 253.
(13) De Paëpe, G.; Giraud, N.; Lesage, A.; Hodgkinson, P.; Böckmann, A.; Emsley, L. *J. Am. Chem. Soc.* **2003**, *125*, 13938.
(14) Hodgkinson, P. *Prog. Nucl. Magn. Reson. Spectrosc.* **2005**, *46*, 197.
(15) Sperling, L. J.; Nieuwkoop, A. J.; Lipton, A. S.; Berthold, D. A.; Rienstra, C. M. *J. Biomol. NMR* **2010**, *46*, 149.
(16) Zorin, V. E.; Brown, S. P.; Hodgkinson, P. *J. Chem. Phys.* **2006**, *125*, 144508.
(17) Akbey, U.; Lange, S.; Trent Franks, W.; Linser, R.; Rehbein, K.; Diehl, A.; van Rossum, B. J.; Reif, B.; Oschkinat, H. *J. Biomol. NMR* **2010**, *46*, 67.
(18) Hologne, M.; Chevelkov, V.; Reif, B. *Prog. Nucl. Magn. Reson. Spectrosc.* **2006**, 48.
(19) Morcombe, C. R.; Gaponenko, V.; Byrd, R. A.; Zilm, K. W. *J. Am. Chem. Soc.* **2005**, *127*, 397.
(20) Mehring, M. *Principles of High Resolution NMR in Solids*; Springer-Verlag: New York, 1983.
(21) Rothwell, W. P.; Waugh, J. S. *J. Chem. Phys.* **1981**, *74*, 2721.
(22) Long, J. R.; Sun, B. Q.; Bowen, A.; Griffin, R. G. *J. Am. Chem. Soc.* **1994**, *116*, 11950.
(23) deAzevedo, E. R.; Saalwachter, K.; Pascui, O.; de Souza, A. A.; Bonagamba, T. J.; Reichert, D. *J. Chem. Phys.* **2008**, *128*, 104505.
(24) Cady, S. D.; Goodman, C.; Tatko, C; DeGrado, W. F.; Hong, M. *J. Am. Chem. Soc.* **2007**, *129*, 5719.
(25) Cady, S. D.; Hong, M. *J. Biomol. NMR* **2009**, *45*, 185.
(26) Su, Y.; Waring, A. J.; Ruchala, P.; Hong, M. *Biochemistry* **2011**, *50*, 2072.
(27) Sakellariou, D.; Brown, S. P.; Lesage, A.; Hediger, S.; Bardet, M.; Meriles, C. A.; Pines, A.; Emsley, L. *J. Am. Chem. Soc.* **2003**, *125*, 4376.
(28) Cadars, S.; Lesage, A.; Emsley, L. *J. Am. Chem. Soc.* **2005**, *127*, 4466.
(29) Duma, L.; Hediger, S.; Brutscher, B.; Böckmann, A.; Emsley, L. *J. Am. Chem. Soc.* **2003**, *125*, 11816.
(30) Lesage, A.; Bardet, M.; Emsley, L. *J. Am. Chem. Soc.* **1999**, *121*, 10987.
(31) Yao, X. L.; Hong, M. *J. Am. Chem. Soc.* **2004**, *126*, 4199.
(32) Bajaj, V. S.; van der Wel, P. C.; Griffin, R. G. *J. Am. Chem. Soc.* **2009**, *131*, 118.
(33) Hong, M.; Griffin, R. G. *J. Am. Chem. Soc.* **1998**, *120*, 7113.
(34) Hong, M.; Su, Y. *Protein Sci.* **2011**, *20*, 641.
(35) Cross, T. A.; Sharma, M.; Yi, M.; Zhou, H. X. *Trends Biochem. Sci.* **2010**, *36*, 117.
(36) Su, Y.; Waring, A. J.; Ruchala, P.; Hong, M. *Biochemistry* **2010**, *49*, 6009.
(37) Hong, M. *J. Magn. Reson.* **1999**, *136*, 86.
(38) Maly, T.; Debelouchina, G. T.; Bajaj, V. S.; Hu, K. N.; Joo, C. G.; Mak-Jurkauskas, M. L.; Sirigiri, J. R.; van der Wel, P. C. A.; Herzfeld, J.; Temkin, R. J.; Griffin, R. G. *J. Chem. Phys.* **2008**, *128*, 052211.
(39) Hu, K. N.; Tycko, R. *Biophys. Chem.* **2010**, *151*, 10.
(40) Carpino, L. A.; Han, G. Y. *Org. Chem.* **1972**, *37*, 3404.
(41) Cady, S., D.; Hong, M. *Proc. Natl. Acad. Sci. U.S.A.* **2008**, *105*, 1483.
(42) Mani, R.; Cady, S. D.; Tang, M.; Waring, A. J.; Lehrer, R. I.; Hong, M. *Proc. Natl. Acad. Sci. U.S.A.* **2006**, *103*, 16242.
(43) Hahn, E. L. *Phys. Rev.* **1950**, *80*, 580.
(44) Hohwy, M.; Rienstra, C. M.; Jaroniec, C. P.; Griffin, R. G. *J. Chem. Phys.* **1999**, *110*, 7983.
(45) Pinto, L. H.; Holsinger, L. J.; Lamb, R. A. *Cell* **1992**, *69*, 517.
(46) Pinto, L. H.; Lamb, R. A. *J. Biol. Chem.* **2006**, *281*, 8997.
(47) Cady, S. D.; Luo, W.; Hu, F.; Hong, M. *Biochemistry* **2009**, *48*, 7356.
(48) Kokryakov, V. N.; Harwig, S. S.; Panyutich, E. A.; Shevchenko, A. A.; Aleshina, G. M.; Shamova, O. V.; Korneva, H. A.; Lehrer, R. I. *FEBS Lett.* **1993**, *327*, 231.
(49) Bellm, L.; Lehrer, R. I.; Ganz, T. *Exp. Opin. Invest. Drugs* **2000**, *9*, 1731.
(50) Tang, M.; Hong, M. *Mol. Biosyst.* **2009**, *5*, 317.
(51) Tang, M.; Waring, A. J.; Hong, M. *J. Am. Chem. Soc.* **2007**, *129*, 11438.
(52) Frankel, A. D.; Pabo, C. O. *Cell* **1988**, *55*, 1189.
(53) Vives, E.; Brodin, P.; Lebleu, B. *J. Biol. Chem.* **1997**, *272*, 16010.
(54) Wang, J.; Qiu, J. X.; Soto, C. S.; DeGrado, W. F. *Curr. Opin. Struct. Biol.* **2011**, *21*, 68.
(55) Tang, M.; Waring, A. J.; Hong, M. *ChemBioChem* **2008**, *9*, 1487.
(56) Khawas, B. *Acta Crystallogr.* **1971**, *B27*, 1517.
(57) Mazumdak, S. K.; Venkatesan, K. *Z. Kristallogr.* **1969**, *130*, 328.
(58) Cowans, B. A.; Grutzner, J. B. *J. Magn. Reson.* **1993**, *105*, 10.
(59) Su, Y.; Doherty, T.; Waring, A. J.; Ruchala, P.; Hong, M. *Biochemistry* **2009**, *48*, 4587.
(60) Petkova, A. T.; Hu, J. G.; Bizounok, M.; Simpson, M.; Griffin, R. G. H., J. *Biochemistry* **1999**, *38*, 1562.
(61) Ladizhansky, V.; Jaroniec, C. P.; Diehl, A.; Oschkinat, H.; Griffin, R. G. *J. Am. Chem. Soc.* **2003**, *125*, 6827.
(62) Rienstra, C. M.; Tucker-Kellogg, L.; Jaroniec, C. P.; Hohwy, M.; Reif, B.; McMahon, M. T.; Tidor, B.; Lozano-Pérez, T.; Griffin, R. G. *Proc. Natl. Acad. Sci. U.S.A.* **2002**, *99*, 10260.
(63) Luo, W.; Cady, S. D.; Hong, M. *Biochemistry* **2009**, *48*, 6361.
(64) Bax, A.; Freeman, R.; Kempsell, S. P. *J. Am. Chem. Soc.* **1980**, *102*, 4849.
(65) Spera, S.; Bax, A. *J. Am. Chem. Soc.* **1991**, *113*, 5490.
(66) Wishart, D. S.; Sykes, B. D.; Richards, F. M. *J. Mol. Biol.* **1991**, *222*, 311.
(67) Levitt, M. H.; Raleigh, D. P.; Creuzet, F.; Griffin, R. G. *J. Chem. Phys.* **1990**, *92*, 6347.
(68) Wang, Y.; Jardetzky, O. *Protein Sci.* **2002**, *11*, 852.
(69) Bajaj, V. S.; Mak-Jurkauskas, M. L.; Belenky, M.; Herzfeld, J.; Griffin, R. G. *Proc. Natl. Acad. Sci. U.S.A.* **2009**, *106*, 9244.
(70) Tang, M.; Waring, A. J.; Lehrer, R. I.; Hong, M. *Angew. Chem., Int. Ed.* **2008**, *47*, 3202.
(71) Rasmussen, B. F.; Stock, A. M.; Ringe, D.; Petsko, G. A. *Nature* **1992**, *357*, 423.
(72) Doster, W.; Cusack, S.; Petry, W. *Nature* **1989**, *337*, 754.
(73) Acharya, A.; Carnevale, V.; Fiorin, G.; Levine, B. G.; Polishchuk, A.; Balannick, V.; Samish, I.; Lamb, R. A.; Pinto, L. H.; DeGrado, W. F.; Klein, M. L. *Proc. Natl. Acad. Sci. U.S.A.* **2010**, *107*, 15075.
(74) Stouffer, A. L.; Acharya, R.; Salom, D.; Levine, A. S.; Di Costanzo, L.; Soto, C. S.; Tereshko, V.; Nanda, V.; Stayrook, S.; DeGrado, W. F. *Nature* **2008**, *451*, 596.
(75) Luo, W.; Hong, M. *J. Am. Chem. Soc.* **2010**, *132*, 2378.
(76) Hu, F.; Luo, W.; Cady, S. D.; Hong, M. *Biochim. Biophys. Acta* **2011**, *1808*, 415.
(77) Li, C.; Qin, H.; Gao, F. P.; Cross, T. A. *Biochim. Biophys. Acta* **2007**, *1768*, 3162.
(78) Fahrner, R. L.; Dieckmann, T.; Harwig, S. S.; Lehrer, R. I.; Eisenberg, D.; Feigon, J. *Chem. Biol.* **1996**, *3*, 543.
(79) Shojania, S.; O'Neil, J. D. *J. Biol. Chem.* **2006**, *281*, 8347.
(80) Wright, P. E.; Dyson, H. J. *J. Mol. Biol.* **1999**, *293*, 321.
(81) Hong, M.; Gross, J. D.; Rienstra, C. M.; Griffin, R. G.; Kumashiro, K. K.; Schmidt-Rohr, K. *J. Magn. Reson.* **1997**, *129*, 85.
(82) De Paëpe, G.; Lesage, A.; Emsley, L. *J. Chem. Phys.* **2003**, *119*, 4833.
(83) Tang, M.; Comellas, G.; Mueller, L. J.; Rienstra, C. M. *J. Biomol. NMR* **2010**, *48*, 103.
(84) Hu, K. N.; Yau, W. M.; Tycko, R. *J. Am. Chem. Soc.* **2010**, *132*, 24.
(85) Mak-Jurkauskas, M. L.; Bajaj, V. S.; Hornstein, M. K.; Belenky, M.; Griffin, R. G.; Herzfeld, J. *Proc. Natl. Acad. Sci. U.S.A.* **2008**, *105*, 883.
(86) Havlin, R. H.; Tycko, R. *Proc. Natl. Acad. Sci. U.S.A.* **2005**, *102*, 3284.
(87) Hu, K. N.; Havlin, R. H.; Yau, W. M.; Tycko, R. *J. Mol. Biol.* **2009**, *292*, 1055.
(88) Siemer, A. B.; Huang, K. Y.; McDermott, A. E. *Proc. Natl. Acad. Sci. U.S.A.* **2010**, *107*, 17580.
(89) Griffin, R. G. *Nature* **2010**, *468*, 381.